

Isotropic and non-diffracting optical metamaterials

T. Paul, C. Menzel, C. Rockstuhl, and F. Lederer

Institute of Condensed Matter Theory and Optics,

Friedrich-Schiller-Universität Jena, Max-Wien-Platz 1, D-07743 Jena, Germany

Abstract

Optical metamaterials have the potential to control the flow of light at will^{1,2,3} which may lead to spectacular applications as the perfect lens⁴ or the cloaking device⁵. Both of these optical elements require invariant effective material properties (permittivity, permeability) for all spatial frequencies involved in the imaging process. However, it turned out that due to the mesoscopic nature of current metamaterials spatial dispersion prevents to meet this requirement⁶; rendering them far away from being applicable for the purpose of imaging^{7,8}. A solution to this problem is not straightforwardly at hand since metamaterials are usually designed in forward direction; implying that the optical properties are only evaluated for a specific metamaterial. Here we lift these limitations. Methodically, we suggest a procedure to design metamaterials with a predefined characteristic of light propagation. Optically, we show that metamaterials can be optimized such that they exhibit either an isotropic response or permit diffractionless propagation.

Metamaterials are usually characterized as deriving their optical properties predominantly from the geometry of subwavelength unit cells and attaining an effective permittivity $\epsilon_{\text{eff}}(\omega)$ or permeability $\mu_{\text{eff}}(\omega)$ not accessible by natural materials. In particular, a sufficient condition for the existence of left-handed waves (wave vector \mathbf{k} is anti-parallel to the Poynting vector \mathbf{S}) as eigenmodes is a negative real part of both effective parameters¹⁰. Then, at normal incidence an effective refractive index, which is defined by normalizing the wavevector by $k_0 = 2\pi/\lambda$, may be introduced and attains negative values, e.g. $n = -1$. Frequently, it is then concluded that such a metamaterial might be employed as a perfect lens¹¹. But this conclusion implicitly assumes that this effective index is invariant for all propagating and evanescent waves.

However, for all current optical metamaterials this requirement is not fulfilled⁷. Most metamaterials perform worse than an ordinary lens since even in the long wavelength limit their refraction, diffraction and absorption properties are anisotropic. Consequently, the effective index is far from being a suitable quantity to describe propagation of light beams of finite spatial width in metamaterials⁸. One rather has to resort to refraction and diffraction coefficients¹³.

Consequently, a reasonable design approach towards metamaterials should not rely on effective material parameters but on desired light propagation characteristics or imaging properties not available in nature. Thus a new design strategy must be developed where a particular optical property of metamaterials represents the essential target function.

Here we show that this design strategy can be based on the dispersion relation of the fundamental Bloch wave which is an eigenmode of a bulk metamaterial. Departing from its dispersion relation $\omega = \omega(k_x, k_y, k_z)$ one can impose desired constraints such as an isotropic optical response (spherical dispersion relation with constant negative curvature) or even a real and imaginary part of the longitudinal wave vector component which does not depend on the transverse one. The former property permits the introduction of a constant effective negative index whereas the latter one causes light to propagate diffractionless at a constant attenuation, rendering the material amenable to a light tunneling scheme for the purpose of imaging^{14,15}. To achieve these design goals the number of degrees of freedom defining a metamaterial has to be increased. Numerical optimization techniques may be subsequently applied to reveal an optimum set of parameters such that the optical response of the metamaterial matches with sufficient precision the predefined one.

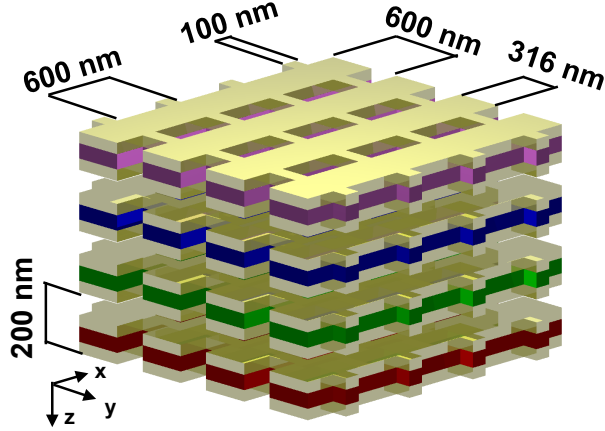


FIG. 1: Artistic view of the supercell metamaterial. The geometrical parameters explicitly stated were kept constant throughout the manuscript. Parameters subject to modifications are the thicknesses of the metallic layers and the thicknesses and the permittivity of the dielectric spacers. The latter are indicated by colors and serve to identify the different functional layers in the super cell. The principal propagation direction is z , the incident field is TE (y) polarized with no variation in y -direction.

These additional degrees of freedom are introduced here by considering metamaterials composed of supercells. The relevant geometry is shown in Fig. 1. A supercell is formed by four functional layers in z direction. Each functional layer consists of two metallic layers separated by a dielectric spacer and is periodic in the transverse x and y directions. The functional layers are distinguished by slightly different layer thicknesses and dielectric constants of the spacer. Each functional layer exhibits the fishnet structure where the geometrical data is taken from literature¹⁶. The fishnet is promising since it allows observing left-handed waves at reasonable low dissipation¹⁷. Furthermore, it can be fabricated by using existing nanotechnology as a bulk material consisting of many functional layers¹⁸. This technology permits for a variation of the optical properties of subsequent layers¹⁹ as required in our approach. In what follows we optimize the additional free parameters (thicknesses, dielectric constant of spacer) such that the metamaterial exhibits the predefined optical properties. We present examples for two relevant cases. The first concerns the design of a metamaterial exhibiting a dispersion relation with a circular iso-frequency curve being equivalent to an effective medium with $n_{\text{eff}}(k_x, k_y) \approx -1$ and the second a metamaterial where light propagates diffractionless.

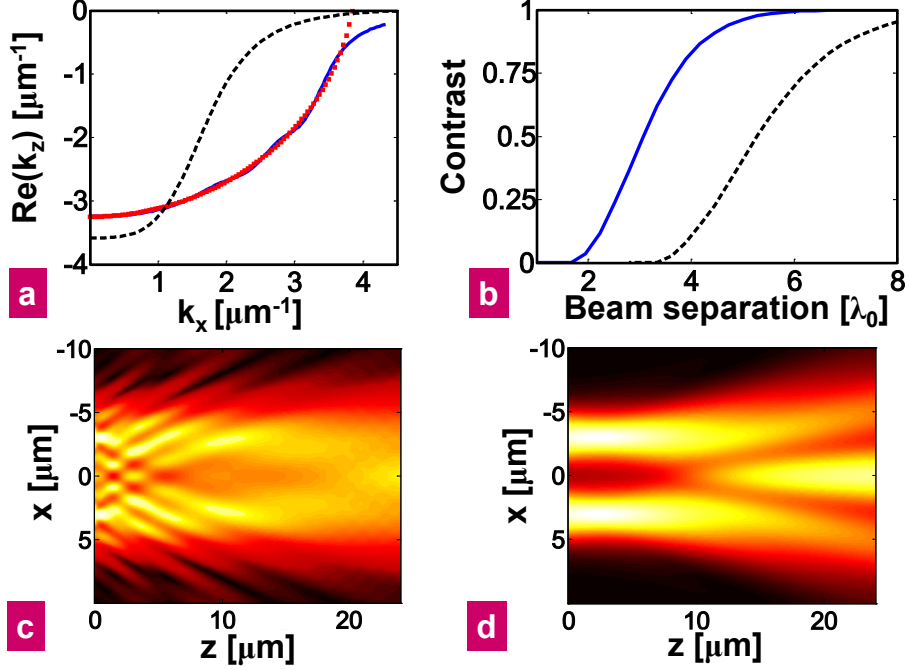


FIG. 2: (a) Real part of the longitudinal wavevector component k_z as a function of the transverse wave vector component k_x (iso-frequency contour) for the original fishnet (black dashed line) and the optimized supercell (blue solid line). The best circular fit is superimposed (red dotted line). (b) The emerging contrast in the object plane upon imaging of two Gaussian beams as function of their initial separation (original fishnet - black dashed line; super cell - blue solid line). (c) Field distribution behind the exit facet of a $2.4 \mu\text{m}$ thick fishnet MM slab (three supercells) if two closely spaced Gaussian beams are placed with their waist in the object plane ($-1.2 \mu\text{m}$) and for a separation of $6 \mu\text{m}$; (d) same scenario but with an optimized super cell .

For referential purpose Fig. 2(a) shows the real part of k_z as a function of k_x at a fixed wavelength ($\lambda = 1.44 \mu\text{m}$) for the original fishnet structure where all functional layers are identical¹⁶. All simulations are performed using a plane wave expansion technique (see Appendix AI). Material properties for silver were taken from literature²⁰. The incident field is TE polarized along the y direction; being the proper polarization for the fishnet to show the desired resonant behavior. The fishnet is neither expected to operate for TM polarization nor for wave fields spatially confined in y direction. The thicknesses of the metal and the dielectric layers were $h = 45 \text{ nm}$ and $h = 30 \text{ nm}$, respectively. The permittivity of the dielectric spacer was $\epsilon = 1.90$. Subsequent functional layers are separated by air; an assumption which is not essential and is lifted below. From Fig. 2(a) it is evident that

the medium is anisotropic but neither uni- nor biaxial because spatial dispersion strongly affects light propagation. Most detrimental for the imaging purpose is the change in sign of the curvature of the iso-frequency contour at $k_x = 1.6 \mu\text{m}^{-1}$. At this inflection point diffraction changes from anomalous to normal preventing reasonable imaging since a lens must compensate for the normal diffraction in free space by a suitable anomalous diffraction. This is proven by imaging two finite Gaussian beams where the image contrast quickly deteriorates with smaller separation (see Fig. 2(b)). Details on the calculation can be found in Appendix AIV. The appearance of normal diffraction for higher spatial frequencies as well as the angular dependent absorption limits the resolution of the metamaterial slab to only $4\lambda_0$.

Now by applying numerical routines (see Appendix AII) we optimized the thicknesses of the metal and the dielectric layers in each functional layer individually. The first target function was a circular iso-frequency contour for the real parts of the wavevector; comparable to that of an isotropic medium with $n = -1$. All geometrical parameters of the optimized structure are documented in Appendix III. The resulting iso-frequency curve along with a best circular fit is shown in Fig. 2(a). The effective index of the medium corresponding to the radius of the best fit amounts to $n_{\text{eff}} = -0.92$. We note that although the medium acts optically isotropic, the geometry of the unit cell is not. Optical isotropy is achieved by globally balancing the spatial dispersion in each functional layer such that all together it effectively disappears. The contrast of two Gaussian beams imaged by this optimized metamaterial slab is shown in Fig. 2(b). Resolution is almost doubled, though it is not yet sub-wavelength. Predominant reason for this is the yet remaining angular dependent absorption. However, this restriction can be lifted by imposing further constraints; as shown below. The superiority of the supercell metamaterial over the conventional is shown in Figs. 2(c) and (d), where the field distributions behind a $2.4 \mu\text{m}$ slab are shown if two closely spaced Gaussian beams are imaged. The waist width ($1/e$ - descent) of the Gaussian beams was $4\lambda_0/(2\pi) = 0.91\mu\text{m}$ each and their separation amounted to $6\mu\text{m}$. The waists are located $1.2 \mu\text{m}$ in front of the slab. As can be seen, for the ordinary fishnet the spots are not resolved whereas the supercell fishnet allows for their clear imaging in the anticipated focal position $1.2 \mu\text{m}$ behind the slab.

To verify that the constraints imposed on the optical performance can be rather freely chosen we detail a second example. Now the target function is a longitudinal wave vector

component (real and imaginary part of k_z) that is independent of the transverse component k_x leading to diffractionless propagation. To ensure that the optimized supercell may be technologically implemented, we choose $\text{Al}_x\text{Ga}_{1-x}\text{As}$ as the dielectric spacer material²¹. Now subsequent functional layers are separated by a polymer with $\epsilon = 2.4$ already used in fabricating stacked metamaterials¹⁹. The thickness of the $\text{Al}_x\text{Ga}_{1-x}\text{As}$ layer was 40 nm. Its permittivity was allowed to vary in the range $\epsilon = 8.41\dots 11.42$. This variation is achievable by a proper stoichiometric ratio of aluminium and gallium. Another free parameter to be optimized was the thickness of the metal layers. Wavelength of operation was $1.56\mu\text{m}$.

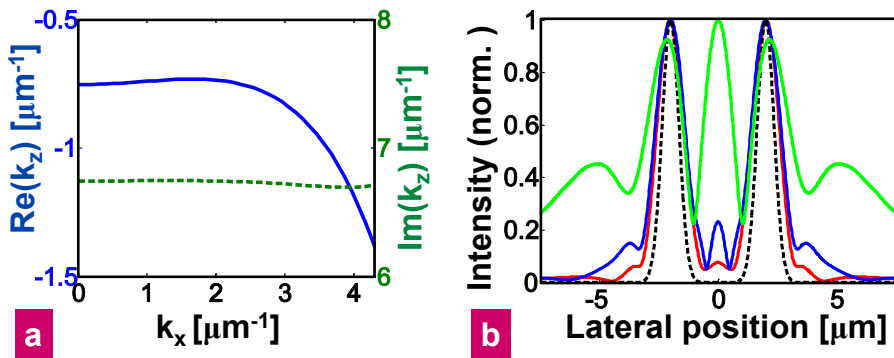


FIG. 3: (a) Real (blue solid line) and imaginary (green dashed line) part of the longitudinal wavevector k_z as function of the transverse wave vector component k_x (iso-frequency contour) for the optimized super cell. Target function of the optimization was an angle independent propagation constant. (b) Field at the exit facet of a $2.4\mu\text{m}$ (red solid line; three supercells) and of a $4.8\mu\text{m}$ (blue solid line; six supercells) if two closely spaced Gaussian beams (separation is $4\mu\text{m}$) are placed at the entrance facet (black dashed line). For comparison the field distribution upon free space propagation over a distance of about $4.8\mu\text{m}$ is also shown (green solid line).

The optimized iso-frequency curves are shown in Fig. 3(a). All geometrical details are documented in Appendix III. It can be seen, that the imaginary part is almost constant, whereas the real part is sufficiently constant up to $\approx 2.5\mu\text{m}^{-1}$. If both quantities would be invariant, each component of the plane wave spectrum of a finite object would exhibit the same phase advance and dissipation upon traversing the metamaterial slab, hence the field distribution at the entrance and exit facet of the metamaterial would be identical.

A verification of almost diffractionless propagation through the optimized metamaterial is documented in Fig. 3(b). There, two closely spaced Gaussian beams (width $1.0\mu\text{m}$) were

placed at the entrance facet of the metamaterial. The field distribution at the exit facet for a metamaterial thickness of $2.4 \mu\text{m}$ and of $4.8 \mu\text{m}$ shows only negligible distortions due to normal diffraction for high spatial frequencies. When compared to the field distribution upon free space propagation, it is evident that diffraction is arrested. Details of the field evolution are documented in Appendix V.

In conclusion, we have shown that metamaterials can be tailored to exhibit certain optical functionalities inaccessible with natural occurring materials. Rather than meaningless effective material parameters the dispersion relation of Bloch waves constitutes the quantity on which constraints are imposed. Here the optimization procedure has been carried out to achieve either an almost perfect, but to date no subwavelength, imaging or diffractionless propagation through a metamaterial. We stress that different target functions can be easily chosen. The required, optimized metamaterials can be fabricated with standard planar technologies already at hand. Constraints imposed on the two-dimensional iso-frequency curve in the current work are only due to the finite computational resources; but in principle they can be imposed on the three-dimensional iso-frequency curve and even on the full dispersion relation. Then one ultimate goal can be achieved, namely the propagation of a light bullet where spreading in space and time is arrested. The ability to mould the flow of light as revealed in this contribution is only a prelude of a genuine class of metamaterials studies that are about to follow.

Acknowledgements

This work was partially financially supported by the Federal Ministry of Education and Research (project Metamat), the Deutsche Forschungsgemeinschaft (Grant No. RO 3640/1-1) and the Thuringian State Government (project Mema).

Appendix

AI Plane wave expansion technique

All simulations in this work were performed by using a home-made code that computes the dispersion relation for a unit cell periodically arranged in the three dimensional space. It takes explicit advantage of this periodicity by expanding all fields and the structure into a plane wave basis. The computation consists of two steps. At first the unit cell is reduced to a certain number of finite layers in which the permittivity is invariant along a predefined principal propagation direction. The eigenmodes propagating in each layer are then solved for by a devoted eigenvalue problem^{22,23}. Assembling these solutions in a scattering matrix and solving for eigensolutions of this scattering matrix allows to find the longitudinal component of the wave vector (propagation constant) of the Bloch eigenmodes as a function of the frequency and the transverse wave vector component²⁴. In our simulations 25x25 plane waves were retained in the simulation; ensuring sufficient numerical accuracy. The advantage of this method is the simple physical interpretation of the propagation constant as a measure for the phase advance of an eigenmode along the propagation direction. The number of modes one solves for is related to the number of plane waves retained in the expansion. In the analysis, only the eigenmode with the lowest imaginary part of the propagation constant is considered. It will dominate the light transport since all other modes suffer a strong absorption. All propagation constants appear as pairs with the same magnitude but opposite sign in the real as well as in the imaginary part; reflecting a forward and a backward propagating wave. For preventing unphysical solutions, one has to choose only that eigenmode which ensures an exponentially decaying solution. Opposite sign in the real and the imaginary part signify an opposite phase and group velocity. Reflection and transmission from a finite slab are computed by imposing usual boundary conditions instead of Bloch periodic boundaries on the fields in the different spatial domains constituting the problem. They are the incident and the transmitted region (eigenmodes are plane waves) and the periodic region (eigenmodes are Bloch modes). Illumination of the structure by finite beams, such as Gaussians, is modeled by decomposing the illumination into a set of plane waves and propagating each plane wave individually.

AII Optimization routines

Having in mind that the spatial dispersion in each functional layer of the super cell shall be

compensated to achieve a predefined dispersion relation, we computed at first the respective dispersion relations for an individual functional layer depending on a single characteristic parameter, such as the thickness of the dielectric intermediate layer or the thickness of the metallic layers while keeping all the other parameters constant. From these solutions a first qualified guess for the arrangement of the functional layers in the super cell could be derived by enforcing that the mean of the dispersion relation matches the predefined criteria. However, this rather simplistic approach does not provide satisfying results; but serves only for the purpose to generate an initial set of data for the subsequent optimization. For this purpose a nonlinear least-squares optimization method (subspace trust-region algorithm based on the interior-reflective Newton method²⁵) was used to optimize the free parameters in the geometry. By relying on the qualified guess about 15 iterations (which correspond to 135 evaluations of the structure’s response) were usually required to approach the optimized solutions. We note that slightly deviating initial conditions might lead to different solutions for the geometrical parameters which do allow, however, for the same dispersion relation.

AIII Detailed structural parameters

Here we provide detailed information on the precise structural parameters of the optimized metamaterials yielding i) an isotropic (imaging) or ii) flat iso-frequency curve (diffractionless propagation). In both cases each supercell consists of four functional layers of $0.2 \mu\text{m}$ constant thickness with slightly different structural parameters given in the tables below. The entire metamaterial slab consists of three supercells such that the overall slab thickness amounts to $2.4 \mu\text{m}$. The metallic layers consist of silver, whereby the dielectric spacer (the layer in between the two metallic layers) is MgF_2 with $\epsilon = 1.90$ in case i) and it is $\text{Al}_x\text{Ga}_{1-x}\text{As}$ in case ii). The permittivity of $\text{Al}_x\text{Ga}_{1-x}\text{As}$ was taken from literature and varies in the range $\epsilon = 8.41 \dots 11.42$ according to the chosen stoichiometric ratio x . The remaining space within the unit cell is only suggested to be completed by a polymer ($\epsilon = 2.40$) in case ii).

AIV Imaging properties

The imaging properties of a metamaterial slab were evaluated by illuminating the structure by two spatially separated Gaussian beams. To calculate the transmitted field behind the slab, the illuminating field was decomposed into its plane wave spectrum and each plane wave was propagated through the structure as described in Appendix AI section. The waist position was located $1.2 \mu\text{m}$ in front of the metamaterial slab. This position exactly corresponds to the front-side focus of a perfect lens with $n = -1$ and a thickness of $2.4 \mu\text{m}$.

| #layer | thickness of metal | thickness of dielectric spacer | permittivity of dielectric spacer |
|--------|-----------------------|-----------------------------------|--------------------------------------|
| 1 | 75.0 nm | 29.7 nm | 1.90 |
| 2 | 72.4 nm | 27.9 nm | 1.90 |
| 3 | 74.1 nm | 26.0 nm | 1.90 |
| 4 | 76.9 nm | 24.2 nm | 1.90 |

TABLE I: Structural parameters of the optimized metamaterial which exhibits a spherical angular dispersion relation.

| #layer | thickness of metal | thickness of dielectric spacer | permittivity of dielectric spacer |
|--------|-----------------------|-----------------------------------|--------------------------------------|
| 1 | 49.8 nm | 40.0 nm | 9.21 |
| 2 | 52.1 nm | 40.0 nm | 9.70 |
| 3 | 33.4 nm | 40.0 nm | 11.05 |
| 4 | 34.3 nm | 40.0 nm | 11.06 |

TABLE II: Structural parameters of the optimized metamaterial which exhibits diffractionless propagation.

These dimensions match nearly that of the optimized metamaterial which consists of three supercells (12 functional layers of thickness $0.2 \mu\text{m}$ each) and which exhibits an effective refractive index of $n_{\text{eff}} = -0.92$ (see main text body for reference).

The field distribution of the electrical field at the waist position is given by

$$E_y(x; z = -1.2\mu\text{m}) = \exp\left[-\frac{(x - S_x)^2}{\sigma^2}\right] + \exp\left[-\frac{(x + S_x)^2}{\sigma^2}\right] \quad (1)$$

with the waist width 2σ and the beam separation $2S_x$. To quantify the resolution limit of a metamaterial lens the beam separation $2S_x$ was continuously decreased whereby the waist width was kept constant with a reasonable value. Now, tracing the field in the focus position (x_f, z_f) allows to evaluate the imaging contrast by

$$C = \frac{|E_y(x_f, z_f)|^2 - |E_y(0, z_f)|^2}{|E_y(x_f, z_f)|^2 + |E_y(0, z_f)|^2}. \quad (2)$$

Of course, in general there exist two foci at (x_f, z_f) and $(-x_f, z_f)$, but because of the symmetry of the illuminating field they are identical. The waist width of the Gaussian

beams was chosen to be $4\lambda_0/(2\pi) = 0.91 \mu\text{m}$ in case of the optimized structure. Further decreasing this size only negligibly affects the transmitted field, since the remaining angular dependent absorption of the metamaterial acts as a low pass filter and therefore it limits the smallest achievable feature size in transmission. Evaluating the imaging contrast of the original fishnet structure the waist width of the Gaussian beams was set to $12\lambda_0/(2\pi) = 2.75 \mu\text{m}$. Otherwise the introduced beam distortions in the transmitted field become too large and a clear determination of the backside foci becomes impossible.

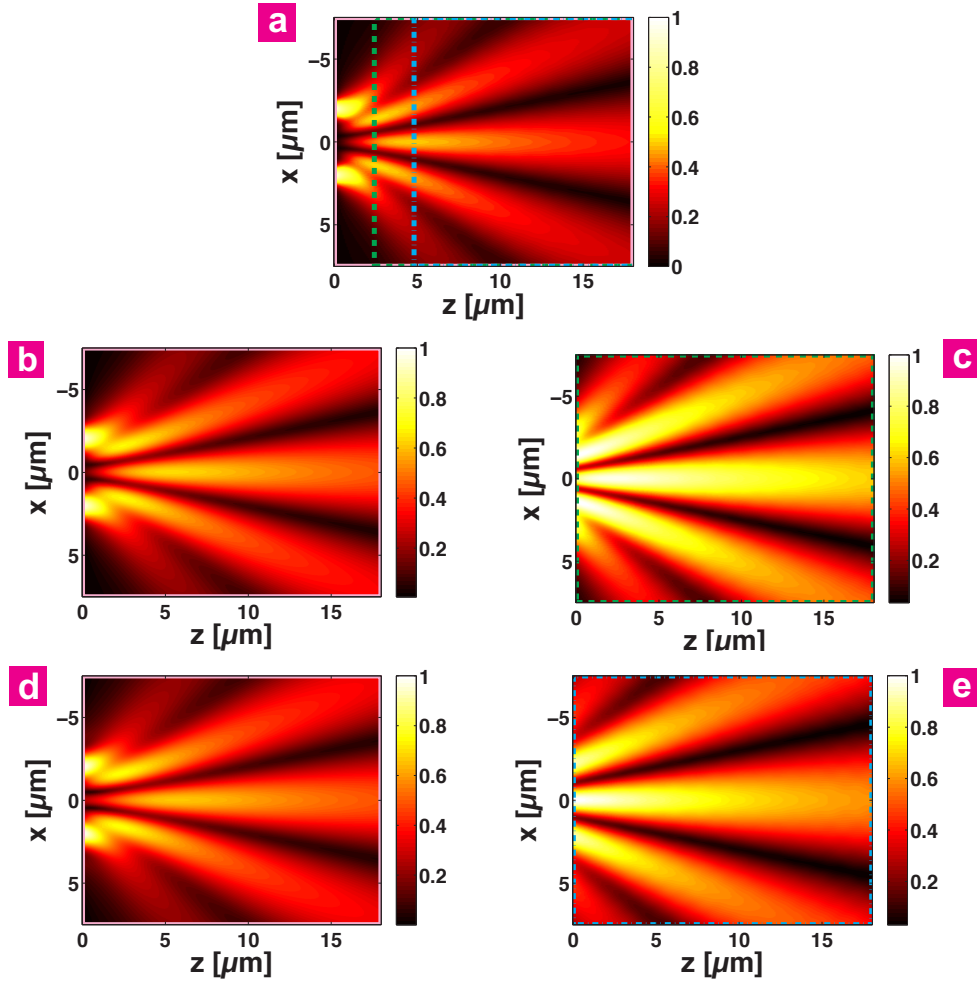


FIG. 4: (a) The normalized electrical field amplitude of a double peak Gaussian source (waist width $4\lambda_0/(2\pi) = 1.0 \mu\text{m}$) during propagation in air at a wavelength $1.56 \mu\text{m}$ for referential purpose. The beam separation is $4 \mu\text{m}$. The waist is located at $z = 0$. By inserting the optimized metamaterial slab structure of thickness (b) $2.4 \mu\text{m}$ and (d) $4.8 \mu\text{m}$ diffraction is suppressed and the propagating field distribution directly behind the exit facet ($z = 0$) changes only negligibly when compared to figure (a). The field plots in figure (c) and (e) show for comparison the case, when the metamaterial slab is removed and the field propagates the same distance of $2.4 \mu\text{m}$ and $4.8 \mu\text{m}$ in free space, respectively. The colored boxes indicate sections of associated field distributions.

-
- ¹ Shelby, R. A., Smith, D. R. & Schultz, S. *Science* 292, 77-79 (2001).
- ² Soukoulis, C. M., Linden, S. & Wegener, M. *Science* 315, 47-49 (2007).
- ³ Shalaev, V. M. *Nature Photon.* 1, 41-48 (2007).
- ⁴ Smith, D. R., Pendry, J. B. & Wiltshire, M. C. K. *Science* 305, 788-792 (2004).
- ⁵ Leonhardt, U Optical Conformal Mapping. *Science* 312, 1777-1780 (2006).
- ⁶ A. Serdyukov, I. Semchenko, S. Tretyakov & A. Sihvola, *Electromagnetics of Bi-Anisotropic Materials - Theory and Applications* (Routledge Chapman & Hall, 2001).
- ⁷ Rockstuhl, C., Paul, T., Menzel, C., Pertsch, T. & Lederer, F. *Phys. Rev. B* 78, 155102 (2008).
- ⁸ Paul, T., Rockstuhl, C., Menzel, C. & Lederer, F. *Phys. Rev. B* 79, 115430 (2009).
- ⁹ Veselago, V. G. *Sov. Phys. Usp.* 10, 509-514 (1968).
- ¹⁰ McCall, M. W., Lakhtakia, A. & Weiglhofer, W. S. *Eur. J. Phys.* 23, 353-359 (2002).
- ¹¹ Pendry, J. B. *Phys. Rev. Lett.* 77, 3966-3969 (2009).
- ¹² Menzel, C., Rockstuhl, C., Paul, T., Lederer, F. & Pertsch, T. *Phys. Rev. B* 77, 195328 (2008).
- ¹³ Christodoulides, D. N., Lederer, F. & Silberberg, Y. *Nature* 424, 817-823 (2003).
- ¹⁴ Jacob, Z., Alekseyev, L. V. & Narimanov, E *Opt. Express* 14, 8247-8256 (2006).
- ¹⁵ Salandrino, A. & Engheta, N. Far-field subdiffraction optical microscopy using metamaterial crystals: Theory and simulations. *Phys. Rev. B* 74, 075103 (2006).
- ¹⁶ Zhang, S. *et al. Opt. Express* 14, 6778-6787 (2006)
- ¹⁷ Dolling, G., Klein, M. W., Wegener, M., Schdle, A., Kettner, B., Burger, S. & Linden S. *Opt. Express* 15, 14219-14227 (2007).
- ¹⁸ Valentine, J., Zhang, S., Zentgraf, T., Ulin-Avila, E., Genov, D. A., Bartal, G. & Zhang, X. *Nature* 455, 376-379 (2008).
- ¹⁹ Liu, N. *et al. Nature Mater.* 7, 31-37 (2008).
- ²⁰ The permittivity of silver: $\epsilon_{\text{Ag}} = 1 - \omega_p^2/(\omega^2 + ig\omega)$, with $\omega_p = 1.37 \times 10^{16} \text{s}^{-1}$ and $g = 8.5 \times 10^{13} \text{s}^{-1}$ was taken from Dolling, G., Enkrich, C., Wegener, M., Soukoulis, C. M., & Linden S. *Opt. Lett* 15, 1800-1802 (2007).
- ²¹ Gehrsitz, S. *et al. J. Appl. Phys* 87, 7825-7837 (2000).
- ²² Noponen, E. & Turunen, J. *JOSA A* 11, 2494-2502 (1994).
- ²³ Li, L. *JOSA A* 13, 1870-1876 (1996).

²⁴ Li, Z. Y. & Ho, K. M. *Phys. Rev. B* 68, 245117 (2003).

²⁵ Coleman, T.F. & Li, Y. *SIAM Journal on Optimization* 6, 418-445 (1996).